CRYSTAL GROWTH & DESIGN

Article

pubs.acs.org/crystal

Impact of Systematic Structural Variation on the Energetics of $\pi-\pi$ Stacking Interactions and Associated Computed Charge Transfer Integrals of Crystalline Diketopyrrolopyrroles

Jesus Calvo-Castro,[†] Monika Warzecha,[†] Alan R. Kennedy,[‡] Callum J. McHugh,*[,†] and Andrew J. McLean*[,†]

[†]School of Science, University of the West of Scotland, Paisley, PA1 2BE, U.K.

[‡]Department of Pure & Applied Chemistry, University of Strathclyde, Glasgow G1 1XL, U.K.

Supporting Information

ABSTRACT: Control over solid state structure is critical for effective performance in optoelectronic devices bearing π-conjugated charge mediating organic materials. A series of five structurally related N-benzyl-substituted diketopyrrolopyrroles (DPPs) differing solely in 2 out their 60 atoms were synthesized and crystal structures obtained. Systematic variation of the long axis aligned, $\pi-\pi$ stacks has been identified within the single crystal structure series and intermolecular interaction energies and charge transfer integrals for the $\pi-\pi$ stacks have been computed by means of density functional theory (M06-2X/6-311G(d)). The computed intermolecular interaction energies as well as charge transfer integrals were further investigated utilizing a series of systematically cropped dimer pairs, highlighting the crucial role of the benzyl/halo substitution on stabilization of these $\pi-\pi$ dimers. Two of the DPPs, including a new polymorph of a previously reported structure exhibit twice the intermolecular interaction energy and comparable hole transfer integrals to Rubrene, one of the most efficient hole conducting materials known. The computed properties for all of the $\pi-\pi$ dimer systems reported herein are consistent with trends predicted by a model system. As such these materials show great promise as charge mediators in organic electronic applications and may be exploited in systematic structure activity based investigations of charge transfer theory.

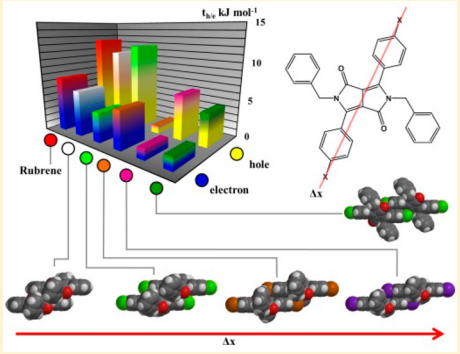

INTRODUCTION

Diketopyrrolopyrrole derivatives are widely employed in the pigment industry[1−3] and have seen an increasing surge of interest as charge transfer mediators in field effect transistors,[4−9] as well as dye-based solar cell technologies.[10−16] We are currently engaged in the development of small molecule diketopyrrolopyrrole platforms in novel optoelectronic and sensing applications. In π-conjugated charge mediating organic systems, crystal engineering by means of control of molecular solid state organization and crystal structure are critical for effective device performance.[17−19] Small changes in molecular structure can have a dramatic impact on those intermolecular electronic interactions which influence key charge transport properties such as charge transfer integrals in organic conducting materials.[20,21] Despite their wide study, there remains an identified need to examine in more detail the impact of systematic structural variation on DPP crystal structures and how that thereby influences the emergence of semiconductor bands in these organic materials.[18] The detailed mechanism accounting for charge transport in organic conducting materials is the subject of considerable debate.[22,23] However, electronic coupling, or charge transfer integrals for hole/electron transport, $t_{h/e}$, play a significant role in all of these treatments. Semiconductor band models[23,24] of charge transport equate the hole or electron bandwidth, $BW_{h/e}$ to $4t_{h/e}$, whereas $t_{h/e}^2$ appears in the pre-exponential factor of thermally activated charge transport models including Marcus Theory.[22] Thus, and led by theoretical treatment of charge transport in organic media, structural control within crystallographic environments leading to large and systematic variation in $t_{h/e}$ is a highly desirable feature of any potential charge mediating organic crystalline system.

In the following, we report the synthesis, determination and characterization of five DPP based crystal structures (Scheme 1 and Figure 1C), that vary systematically on the basis of atom substituents at the para position of the DPP core phenyl ring. The five structures determined were based on hydro (***HBDPP***), chloro (***ClBDPPα*** and ***ClBDPPβ***), bromo (***BrBDPP***), and iodo (***IBDPP***) substituted DPPs as indicated in Scheme 1. Variation of halogen substitution was rationalized upon the enhanced optoelectronic behavior observed in materials containing these groups.[17,25] All of these structures exhibit long molecular axis, slipped, $\pi-\pi$ cofacial stacking motifs which are generally considered to be the key structural features leading to the emergence of semiconductor band structures in organic

Received: July 6, 2014
Published: July 28, 2014

Scheme 1. DPP Synthetic Route[a]

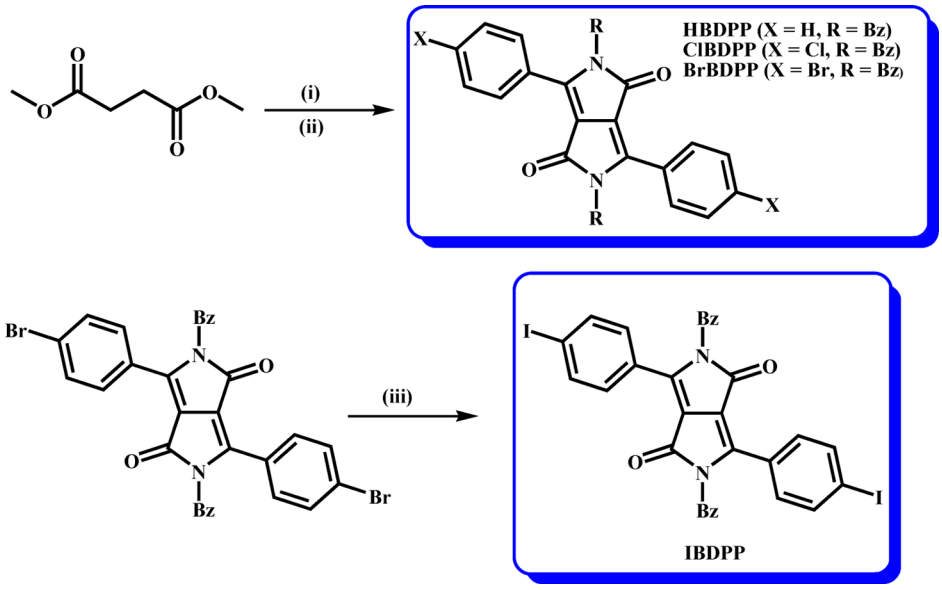

[a](i) PhCNX, Na, *t*-amyl alcohol, 120 °C; (ii) BzBr, K_2CO_3, DMF, 120 °C; (iii) NaI, CuI, DMAc, 165 °C.

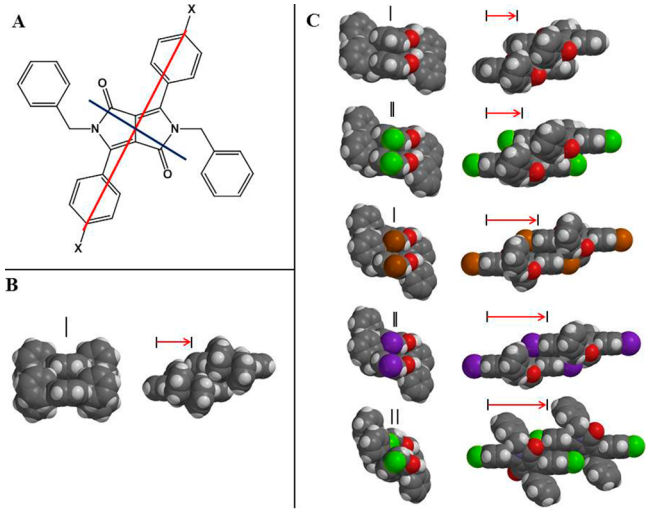

Figure 1. (A) ***XBDPP*** crystal structures determined with short and long molecular axes in blue and red, respectively. (B and C) Long and short molecular axis perspective views of the crystal extracted $\pi-\pi$ overlapped dimers (left and right columns respectively). (B) *b* axis stack Rubrene. (C) Top to bottom: ***HBDPP***, ***ClBDPPβ***, ***BrBDPP***, ***IBDPP***, and ***ClBDPPα***.

crystalline materials.[20,21] The degree of long molecular axis slip and hence charge transfer integral varies systematically with halo substitution on the phenyl groups while the short axis slip is controlled to within 0.3 Å in all but one structure, as opposed to those nonbenzylated diketopyrrolopyrrole analogues.[26,27] The study also establishes a new crystal polymorph of ***ClBDPP*** with significantly different computed electronic properties to that of the crystal structure previously reported[28] (herein denoted as ***ClBDPPα***), representing one of very few examples of polymorphism in N-substituted diketopyrrolopyrrole derivatives.[29] An observation that illustrates the potential for polymorphism induced enhancement of optoelectronic performance in organic devices.[18]

In addition, two of the new crystal structures reported possess computed t_h values comparable to that of Rubrene[30,31] one of the most effective charge carrying organic crystalline materials[32] (which we use as a reference material). Small variations in the intermolecular displacements within the dimers comprising the stacks are responsible for significant changes in the magnitude and character of charge transfer integrals. Consequently, large intermolecular interactions, ΔE_{CP} are highly desirable to preserve the thermal integrity of the 1-D $\pi-\pi$ stacks. However, it is important to establish the nature of the interactions leading to large ΔE_{CP} values; vibrational activation of multiple, individual low energy interactions at room temperature may lead to considerable thermal-induced slippage of the $\pi-\pi$ stacks leading in turn to thermally induced variation in $t_{h/e}$. The optimal hydro and chloro benzyl substituted DPP derivatives investigated exhibit either comparable or twice as large as the computed ΔE_{CP} for the Rubrene dimer in Figure 1B. As a consequence, our results should be of broad interest to those developing crystalline organic electronic materials, particularly those based around the DPP architecture.

EXPERIMENTAL SECTION

Reagents and Instrumentation. Pigment Red 254 and Pigment Red 3100D were kindly obtained from BASF as a gift and used as received. Unless otherwise stated, all other starting materials and reagents were obtained from Sigma-Aldrich and used as received. ^{1}H NMR and ^{13}C NMR spectra were determined using a JEOL ECS400 400 MHz spectrometer (in $CDCl_3$ or DMSO-d_6,). Elemental analyses were carried out using the service provided at Jagiellonian University in Krakow, Poland. FTIR analyses were carried out on the neat samples by attenuated total reflectance using a PerkinElmer, Spectrum One FTIR Spectrometer, with Universal ATR Sampling Accessory.

Synthesis. *3,6-Diphenyldihydropyrrolo[3,4-c]pyrrole-1,4-dione (HDPP).* A mixture of potassium tertiary butoxide (21.04 g, 187 mmol) and benzonitrile (6.36 g, 61 mmol) in anhydrous 2-methyl-2-butanol (10 mL) was heated at reflux temperature. Under vigorous stirring, dimethyl succinate (4.74 g, 32 mmol) was added over 2 h. After it was further stirred for 2 h at reflux temperature, the mixture was cooled to 50 °C and treated with methanol (40 mL) and acetic acid (12 mL). After further cooling to room temperature, the precipitate was collected by filtration with a membrane filter (0.45 μm,

dx.doi.org/10.1021/cg5010165 | *Cryst. Growth Des.* 2014, 14, 4849−4858

Table 1. Selected Crystallographic Data and Refinement Parameters for XBDPP Compounds

	HBDPP	*ClBDPPβ*	*BrBDPP*	*IBDPP*	*ClBDPPα*
formula	$C_{32}H_{24}N_2O_2$	$C_{32}H_{22}Cl_2N_2O_2$	$C_{32}H_{22}Br_2N_2O_2$	$C_{32}H_{22}I_2N_2O_2$	$C_{32}H_{22}Cl_2N_2O_2$
M_r (g mol^{-1})	468.35	537.42	626.34	720.32	537.42
cryst syst	triclinic	monoclinic	monoclinic	monoclinic	monoclinic
space group	$P\bar{1}$	$P2_1/c$	$P2_1/a$	$P2_1/c$	$P2_1/c$
temp (K)	153(2)	100(2)	100(2)	120(2)	100(2)
a (Å)	5.8501(5)	13.237(18)	9.1771(10)	9.4307(8)	8.401(5)
b (Å)	7.8284(6)	15.442(19)	15.0045(18)	13.8089(15)	10.063(6)
c (Å)	13.0761(12)	6.276(8)	9.3642(12)	10.1510(5)	14.799(9)
α (deg)	74.624(8)				
β (deg)	83.442(7)	99.524(18)	97.956(7)	93.843(6)	92.610(6)
γ (deg)	86.913(7)				
V (Å^3)	573.46(8)	1265(3)	1277.0(3)	1318.97(19)	1249.8(13)
Z	1	2	2	2	2
X-ray source	tube	synchrotron	rotating anode	tube	synchrotron
wavelength (Å)	1.5418	0.6889	0.71073	0.71073	0.6889
measured reflns	4553	10080	11464	5597	11910
unique reflns	2231	2274	2240	2907	2833
R_{int}	0.0207	0.1161	0.1151	0.0320	0.0386
observed reflns [$I > 2\sigma(I)$]	1987	1383	1516	2202	2378
μ (mm^{-1})	0.671	0.291	3.208	2.418	0.295
no. of params	163	172	172	172	172
$2\theta_{max}$ (deg)	146.35	49.00	50.00	56.18	53.66
R [on F, obs reflns only]	0.0404	0.0898	0.0684	0.0491	0.0527
wR [on F^2, all data]	0.1113	0.2621	0.1851	0.1236	0.1423
GOF	1.074	1.029	1.001	1.031	1.098
largest diff. peak/hole (e Å^{-3})	0.227/−0.248	0.677/−0.690	0.837/−1.472	1.154/−0.595	0.822/−0.366

ø 47 mm), washed repeatedly with water and dried to give HDPP (2.89 g, 35%) as an insoluble red powder. ^{1}H NMR (DMSO-d_6): 7.58 (6H, m, ArH), 8.43, (4H, m, ArH),11.31, (2H, s, NH). IR (ATR)/cm^{-1}: 3134 (NH), 3049 (ArH), 1648 (C═O), 1641 (NH) 1568 (C═C), 1501 (C═C), 765.15 (ArH), 739.45 (ArH).

*2,5-Dibenzyl-3,6-diphenylpyrrolo[3,4-c]pyrrole-1,4(2H,5H)-dione (**HBDPP**).* A suspension of potassium carbonate (7.00 g, 51 mmol) in DMF (40 mL) was heated at 120 °C. At this temperature under vigorous stirring, HDPP (2.00 g, 6.9 mmol) was added giving a dark violet color. Benzyl bromide (6 mL, 50 mmol) in DMF (10 mL) was dropped into the pigment solution slowly over 40 min. The mixture was stirred at 120 °C for a further 2 h and the color changed to dark orange. The reaction was quenched by cooling to room temperature and adding an ice-cooled methanol−water mixture (100 mL). The precipitate was collected by filtration and washed repeatedly with methanol and water. The crude product was purified by wet flash chromatography, eluting with a gradient of 0−70% hexane in DCM to give ***HBDPP*** (0.8 g, 24%) as an orange powder. ^{1}H NMR ($CDCl_3$): 4.95 (4H, s, CH2), 7.18 (4H, d, ArH), 7.23−7.30 (6H, m, ArH), 7.41−7.46 (6H, m, ArH), 7.73(4H, d, ArH). 13C NMR ($CDCl_3$): 46.0 (CH2), 126.8 (C═C) 127.5 (C═C), 127.9 (C═C), 128.8 (C═C), 128.9 (C═C), 129.1 (C═C), 131.5 (C═C), 137.5 (C═C), 149.1 (C═C), 163.2 (C═O). IR (ATR)/cm^{-1}: 3033 (ArH), 2932 (CH2), 1659 (C═O), 1603 (C═C), 1566 (C═C), 1496 (C═C), 1382 (CH2), 1358 (CH2), 728 (ArH). Anal. Calcd for $C_{32}H_{24}N_2O_2$: C, 82.03; H, 5.16; N, 5.98. Found: C, 81.77; H, 5.21; N, 5.76. Melting point: 278 °C.

*2,5-Dibenzyl-3,6-bis(4-chlorophenyl)pyrrolo[3,4-c]pyrrole-1,4-(2H,5H)-dione (**ClBDPP**).* The procedure was similar to that described for ***HBDPP*** from Pigment Red 254 (0.29 g, 0.81 mmol), K_2CO_3 (1,50 g, 11 mmol) and benzyl bromide (1.19 mL, 10 mmol). The precipitate was collected by filtration and recrystallized from ethanol/DCM to give ClBDPP as an orange/red powder (0.20 g, 45%). ^{1}H NMR ($CDCl_3$): 4.95 (4H, s, CH_2), 7.16 (4H, d, ArH), 7.23−7.32 (6H, m, ArH), 7.41 (4H,d, ArH), 7.70 (4H, d, ArH). ^{13}C NMR ($CDCl_3$): 45.8 (CH_2), 126.2 (C═C), 126.6 (C═C), 127.7 (C═C),129.0 (C═C), 129.3 (C═C), 130.5 (C═C), 137.2 (C═C), 137.8 (C═C), 148.1 (C═C), 162.9 (C═O). IR(ATR)/cm^{-1}: 2947 (ArH), 2923 (ArH), 1670 (C═O), 1613 (C═C), 1586 (C═C), 1500 (C═C), 1376(CH_2), 1355 (CH_2) 834 (ArH), 849, (ArH), 676 (ArH). Anal. Calcd for $C_{32}H_{22}N_2O_2Cl_2$: C, 71.51; H, 4.13; N, 5.21. Found: C, 71.55; H, 4.16; N, 5.11. Melting point: both polymorphs 276−278 °C.

*2,5-Dibenzyl-3,6-bis(4-bromophenyl)pyrrolo[3,4-c]pyrrole-1,4-(2H,5H)-dione (**BrBDPP**).* The procedure was similar to that described for HDPP from Pigment Red 3100D (1.45 g, 3.11 mmol), K_2CO_3 (6.00 g, 43 mmol) and benzyl bromide (4.60 mL, 38 mmol). Recrystallization from hexane gave BrBDPP as a red powder (1.03 g, 50%). ^{1}H NMR ($CDCl_3$): 4.94 (4H, s, CH_2), 7.16 (4H, d, ArH), 7.24−7.30 (6H, m, ArH), 7.56 (4H, d, ArH), 7.63 (4H, d, ArH). ^{13}C NMR ($CDCl_3$): 45.8 (CH_2), 126.3 (C═C), 126.7 (C═C), 127.7 (C═C), 129.0 (C═C), 130.6 (C═C), 132.3 (C═C), 137.2 (C═C), 148.2 (C═C), 162.7 (C═O). IR (ATR)/cm^{-1}: 3031 (ArH), 2990 (CH_2), 1658 (C═O), 1586 (C═C), 1542 (C═C), 1377 (CH_2), 1354 (CH_2), 834 (ArH), 823 (ArH), 695 (ArH), 683 (ArH). Anal. Calcd for $C_{32}H_{22}N_2O_2Br_2$: C, 61.36; H, 3.54; N, 4.47. Found: C, 61.53; H, 3.56; N, 4.58. Melting point: 250 °C.

*2,5-Dibenzyl-3,6-bis(4-iodophenyl)pyrrolo[3,4-c]pyrrole-1,4-(2H,5H)-dione (**IBDPP**).* A mixture of BrBDPP (1.00 g, 1.6 mmol), sodium iodide (3.60 g, 24 mmol), copper(I) iodide (1.52 g, 8 mmol) and dimethylacetamide (35 mL) was stirred under nitrogen at 165 °C for 125 h. The resulting mixture was then cooled to 80 °C and mixed with water (50 mL). The slurry was filtered and washed with water (2 × 30 mL) and ethanol (10 mL), which gave a pink/red powder. The powder was boiled with chloroform and filtered, and then recrystallized from chloroform/hexane to give IBDPP as a red powder (0.19 g, 33%). ^{1}H NMR ($CDCl_3$): 4.94 (4H, s, CH_2), δ 7.16 (4H, d, ArH), 7.24−7.29, (6H, m, ArH), 7.45 (4H, d, ArH), 7.76 (4H, d, ArH). ^{13}C NMR ($CDCl_3$): 45.8 (CH_2), 126.6 (C═C), 127.7 (C═C), 129.0 (C═C), 130.4 (C═C), 130.6 (C═C), 132.3 (C═C), 137.2 (C═C), 138.3 (C═C), 148.3 (C═C), 162.7 (C═O). IR (ATR)/cm^{-1}: 3029 (ArH), 2990 (CH_2), 1659 (C═O), 1610 (C═C), 1585 (C═C), 1537 (C═C), 1490 (CH_2), 832 (ArH), 822 (ArH), 695 (ArH), 674 (ArH). Anal. Calcd for $C_{32}H_{22}N_2O_2I_2$: C, 53.36; H, 3.08; N, 3.89. Found: C, 53.49; H, 3.18; N, 3.98. Melting point: 276 °C.

dx.doi.org/10.1021/cg5010165 | *Cryst. Growth Des.* 2014, 14, 4849−4858

Preparation of Crystals for Single Crystal X-ray Diffraction analysis. ***HBDPP***: Slow evaporation of a cooled solution of ***HBDPP*** in DCM/hexane (1:1). ***ClBDPPα***: Slow evaporation of a cooled solution of ***ClBDPP*** in DCM/hexane (1:1). ***ClBDPPβ***: Slow evaporation of a solution of ***ClBDPP*** in chloroform at room temperature. ***BrBDPP***: Slow evaporation of a cooled solution of ***BrBDPP*** in DCM/hexane (1:1). ***IBDPP***: Slow evaporation of a cooled solution of ***IBDPP*** in DCM/hexane (1:1).

Crystal Structure Determination. Single-crystal data for both Cl polymorphs were measured at Station I19 of the DIAMOND synchrotron light source.[33] Other data sets were measured with laboratory-based instruments using monochromatic radiation. The structures were refined to convergence against F^2 using all independent reflections and by full-matrix least-squares using the program SHELXL-97.[34] Selected parameters are given in Table 1 and full details are given in the deposited cif files. CCDC reference numbers 980388−980392 contain the supplementary crystallographic data for this paper.

Computational Details. All molecular modeling studies were carried out using the density functionals indicated below as implemented in Spartan10 software.[35] Dimer interaction energies, ΔE_{CP}, were all corrected for basis set superposition error (BSSE) using the counterpoise correction method.[36] Using a cutoff distance of van der Waals (VdW) radius +0.3 Å, all nearest neighbor dimer interaction energies of crystal extracted-dimer structures and charge transfer integrals of $\pi-\pi$ dimers were calculated using the M06-2X density functional[37] and 6-311G(d) basis set. This density functional has been shown to give good account of the dimer interaction energies of $\pi-\pi$ interacting systems.[38,39] Charge transfer integrals exhibited little dependence on basis set (6-31G(d), 6-31G(d)(p), 6-31+G(d) and 6-311G(d) were examined). The final choice of 6-311G(d) was based on its suitability for Iodo containing structures. All results in the main text therefore refer to M06-2X/6-311G(d) calculations on crystal derived dimer species.

The computation of the dimer interactions of an **HDPP** model system were performed by means of single point M06-2X/6-31G(d) calculations on a series of **HDPP** model dimers to determine both charge transfer integrals and dimer interaction energies and were carried out as follows: the dimer comprised two M06-2X/6-31G(d) generated **HDPP** monomer structures where the phenyl/DPP torsional angles were constrained to 0°. The two monomers were mutually aligned parallel and directly on top of another with an intermonomer separation distance, Δz = 3.6 Å. Starting from the fully eclipsed structure, Δx = 0, one monomer was shifted relative to the other by a distance Δx in a series of approximately 0.3 Å increments while keeping Δy = 0 and Δz = 3.6 Å. A series of single point, BSSE corrected M06-2X/6-31G(d) dimer interaction energies, ΔE_{CP}, were computed over the full 15.3 Å of Δx slip. No geometry relaxation of the monomers or dimer structures was allowed at any point.

RESULTS AND DISCUSSION

Structural Description. Five single-crystal structures of ***XBDPP*** derivatives where X denotes the substituents on the para position of the phenyl rings on positions 3 and 6 of the DPP core and B represents the N-benzyl substitution, are presented and compared. ***ClBDPP*** was found to exist as two polymorphic forms, the previously described yellow form[28] (hereafter ***ClBDPPα***) and a new red form (hereafter ***ClBDPPβ***). Although single crystal structures of pigment materials are often hard to come by, due largely to the inherent insolubility of these compounds, the current interest in DPP derived materials has led to a number of structural reports. Indeed a search of the CCDC (July 2014 version) found 63 DPP structures with C6 aromatic substituents as per the compounds described here.[40] This included a description of a DMF solvate of ***BrBDPP***.[41] Despite this relative abundance of database structures, the ***XBDPP*** structures reported here are of especial importance as due to the sequential variation of the X groups, they form a rare systematic series of DPP structures. This gives a unique opportunity to probe structure−property relationships in these materials.

All 5 structures have molecules with crystallographically imposed centrosymmetry (Z′ = 0.5) with an inversion center sited in the middle of the transannular C−C bond that is shared by the two 5-membered rings of the DPP core. This is a common structural feature of the symmetrically substituted DPP structures found in the crystallographic database. The bond lengths of the DPP fragments of all the ***XBDPP*** species (including the solvate of ***BrBDPP***) show no chemically significant variations: all are essentially equivalent and thus changing X does not have a measurable effect here. For the ***HBDPP*** and ***ClBDPP*** species, the N atoms are distorted somewhat from planar geometry. This slight pyrimidalization is most noticeable in the displacement of the phenyl C atom bound to N out of the DPP ring plane (by 0.377(2), 0.319(4), and 0.294(9) Å for ***HBDPP***, ***ClBDPPα*** and ***ClBDPPβ***, respectively). This effect is smaller for the heavier analogues (0.151(12) and 0.066(8) Å for ***BrBDPP*** and ***IBDPP***, respectively) a sequence that is suggestive of a systematic change. This distortion appears to be correlated with a change in dihedral angle between the planes of the DPP and benzyl rings. These angles are 77.67(7)°, 76.81(19)°, 85.3(3)°, 88.9(3)°, and 79.36(9)° for the ***HBDPP***, ***ClBDPPβ***, ***BrBDPP***, ***IBDPP*** and ***ClBDPPα*** substituted species. Thus, more perfectly planar N atoms are associated with more perfectly perpendicular dihedral angles.

Comparing polymorphs ***ClBDPPα*** and ***ClBDPPβ***, a clear difference in molecular conformation is apparent as illustrated in Figure 2. For the α form the chlorobenzene ring is twisted much further out of the DPP ring plane than is the case for the β form (compare torsion angles of 44.0(3)° and 20.0(7)°). All the other ***XBDPP*** structures have smaller twists, in line with that of the β form (range 20.6(10)−22.5(2)°). The slightly more dense α form is thus the outlier here. Analyzing the structures found in the database search shows that the α form is unusual in a wider sense too. The equivalent torsion angles in the database search ranged from 0° to 65°, however all other structures with large torsion angles (approximately 35−65°)

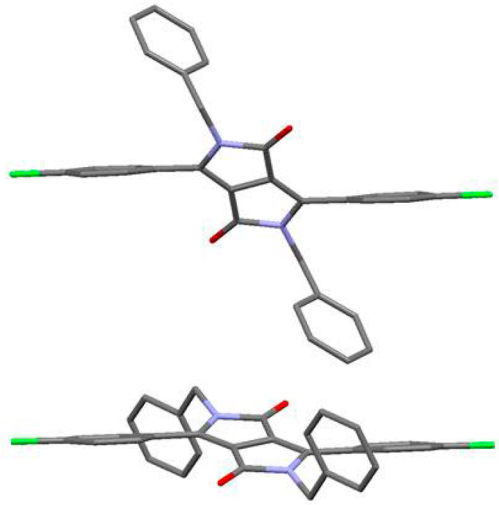

Figure 2. Molecular structures of ***ClBDPPα*** (above) and ***ClBDPPβ*** (below) drawn with C_6H_4Cl rings perpendicular to the page so as to emphasize the difference in molecular conformation.

dx.doi.org/10.1021/cg5010165 | Cryst. Growth Des. 2014, 14, 4849−4858

involved aromatic C6 rings with sterically demanding ortho substituents. ***ClBDPPα*** is thus unusual in its color (yellow versus red in the β form), in its molecular conformation and in its intermolecular packing.

Each packing structure can be described as π stacked along a crystallographic axis (a for ***HBDPP*** and ***BrBDPP***, b for ***ClBDPPα***, and c for ***ClBDPPβ*** and ***IBDPP***) with short contacts formed between the DPP and C_6H_4X rings (for example C···C separations of 3.345 Å in ***HBDPP***, see Figure 3). As cofacial

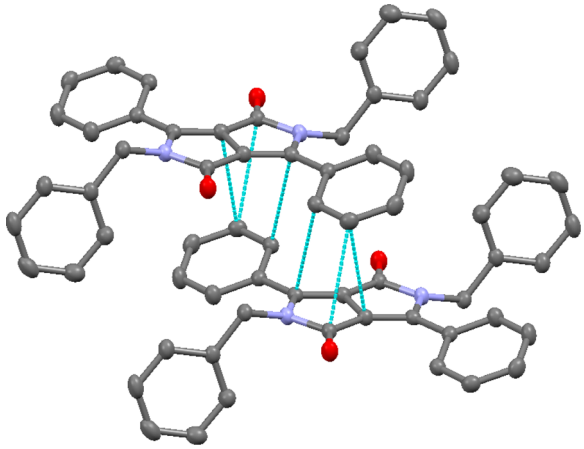

Figure 3. Dimeric pair of molecules from ***HBDPP*** showing the closest $\pi-\pi$ cofacial contacts as light blue dotted lines.

$\pi-\pi$ stacks are of great importance in developing semiconductor bandwidth in crystalline organic materials, they were subject to further investigation and are described below in terms of a long molecular axis (the X to X vector incorporating the longest π system) and a short axis running between the benzyl rings, see Figure 1A.

Intermolecular Interaction Energies, ΔE_{CP}. To probe thermal integrity and dimer stability we calculated the intermolecular interaction energies. All the nearest neighbors (within a distance equal to that of the van der Waals radius +0.3 Å for all the ***XBDPP***s were identified and their dimer interactions energies, ΔE_{CP} computed (refer to Supporting Information for full details). It is noteworthy that the $\pi-\pi$ dimers in Figure 1C exhibit the strongest nearest neighbor dimer interaction energies of all the respective structures. If it is assumed that ΔE_{CP} for all of the individual dimers are determined by local interactions, then the relative thermal stability of the various crystal structures can be estimated based on the sum of all of the ΔE_{CP}s from nearest neighbor dimer interactions. We find then that total binding energy of the α and β forms of ***ClBDPP*** are effectively identical; −263 and −264 kJ mol^{-1} respectively (as were their melting points; 276−278 °C). The β form has 8 nearest neighbors versus 12 for the α form, thus the large $\pi-\pi$ dimer ΔE_{CP} of the β (−69.6 kJ mol^{-1}) versus the α (−42.5 kJ mol^{-1}) polymorph is offset by the larger number of weaker nearest neighbor dimer interactions associated with the latter's crystal structure. The largest and lowest total interaction energies were found for ***HBDPP*** (−294 kJ mol^{-1}) and ***BrBDPP*** (−253 kJ mol^{-1}) respectively which also crudely reflect their respective melting points of 278 and 250 °C. Explicit thermal analysis would clearly be of interest here and will feature in later studies of these systems.

Given the key role of the $\pi-\pi$ stacking motif in mediating charge transfer processes in organic materials,[31,38,42] we concentrate the remainder of our discussion on these dimer pairs. Spaced filled structures for these dimers are given in Figure 1B (for Rubrene[30]) and 1C (for ***XBDPP***s) from the perspective of the long and short molecular axis, x and y respectively. Dimer interaction energies, ΔE_{CP} of −70.2, −69.9, −39.5, −35.5, and −42.5 kJ mol^{-1} were computed for ***HBDPP***, ***ClBDPPβ***, ***BrBDPP***, ***IBDPP***, and ***ClBDPPα***. These are either comparable or twice as large as −35.6 kJ mol^{-1} obtained for the Rubrene $\pi-\pi$ cofacial dimer in Figure 1B, suggesting that the thermal integrity of the ***HBDPP*** and ***ClBDPPβ*** 1-D $\pi-\pi$ stacks may be greater than that of the Rubrene stack. Furthermore, these large interaction energies for $\pi-\pi$ cofacial systems are somewhat at odds with recent suggestions in the literature that such interactions in DPP based systems are weak.[43] Instead we find that they represent the strongest dimer interactions of all in our systems. Large intermolecular interaction energies and the consequent high thermal integrity represent a highly desirable feature in organic charge transfer mediators in regards to the sensitivity of $t_{h/e}$ to small intermolecular displacements,[20,21,42] so the significant interaction energies obtained here relative to Rubrene are of particular note.

The most striking feature of the ***XBDPP*** $\pi-\pi$ dimers is the systematic and progressive increase of the intermonomer displacement over the long molecular axis, Δx, with increasing size of the halogen ranging from 4.5, 5.1, 8.4, and 9.4 Å for ***HBDPP***, ***ClBDPPβ***, ***BrBDPP***, and ***IBDPP*** respectively (Figure 1C). Concomitant displacements along the short molecular, y, axis are relatively invariant, $0.0 < \Delta y < 0.3$ Å in these ***XBDPP*** systems. The exception to this strong Δy alignment is the ***ClBDPPα*** polymorph (which also exhibits a different molecular conformation to the others) where $\Delta x = 9.4$ Å and $\Delta y = 1.3$ Å. Vertical, Δz, displacements as defined by the distance between xy planes of the two comprising monomers are all within VdWs contact and are of the order of 3.2−3.5 Å. To rationalize the effects of substitution in developing this strong alignment along the short molecular axis as well as the effect of the benzyl groups in these ***XBDPP*** systems, the crystal structures of the nonbenzylated analogues, namely ***HDPP***[27] and ***ClDPP***[26] were downloaded and $\pi-\pi$ stacked dimers extracted from the CCDB. These exhibit two $\pi-\pi$ stacking interactions each per molecule as opposed to their benzylated counterparts. For ***HDPP***, these are associated with Δx, Δy, and Δz of 0.7, 1.8, 3.5 Å and 1.9, 5.6, 2.9 Å respectively. For ***ClDPP*** Δx, Δy and Δz are observed of 3.4, 3.0, 3.1 and 2.3, 4.3, 3.2 Å, respectively; Δy consistently exceeds those reported here for the associated ***XBDPP***s indicating the influence of the benzyl substituents in restricting the displacement along the short molecular axis in at least two of the five dimers in Figure 1C. This Δy restriction has also been the case in other structural analogues incorporating solubilizing alkyl chains instead of benzyl groups.[43] The role of the substituents, both halogen atoms and benzyl groups, in controlling the displacements along the long and short molecular axis respectively, was examined through a series of ΔE_{CP} calculations on various *cropped* ***XBDPP*** dimers.

In Table 2 we use bold italics to denote intact, ***XBDPP*** crystal $\pi-\pi$ dimers as listed in Figure 1 and bold for the derived, cropped structures. Halogen substituents and benzyl groups were cropped out and replaced with H atoms individually and then simultaneously yielding **BDPP**, **XDPP**, and **DPP** cropped $\pi-\pi$ dimers, respectively. The intermolec-

dx.doi.org/10.1021/cg5010165 | Cryst. Growth Des. 2014, 14, 4849−4858

Table 2. Counterpoise-Corrected Interaction Energies for Structurally Modified and Non-Structurally Modified $\pi-\pi$ Dimers of Different N-Benzyl-Substituted DPP Derivatives (M06-2X/6-311G(d))

compound	XBDPP (kJ mol^{-1})	XDPP (kJ mol^{-1})	BDPP (kJ mol^{-1})	DPP (kJ mol^{-1})
HBDPP	−70.1	−41.9	−70.1	−41.9
ClBDPPβ	−69.9	−51.2	−64.6	−41.9
BrBDPP	−39.5	−34.4	−23.4	−21.7
IBDPP	−35.5	−30.7	−12.01	−11.7
ClBDPPα	−42.5	−41.2	−29.7	−29.6

ular interaction energies are summarized in Table 2 for these dimer pairs.

On the basis of the difference between ΔE_{CP} values of the **BDPP** and **DPP** pairs, it can be seen that the benzyl groups appear to play a significant role in stabilization of the DPP cores in the ***HBDPP*** and ***ClBDPPβ*** $\pi-\pi$ dimers, but not in those of ***BrBDPP***, ***IBDPP*** and ***ClBDPPα***. There are three local, benzyl based contributing interactions responsible for the stability imparted into the ***HBDPP*** and ***ClBDPPβ*** $\pi-\pi$ dimer pairs; cofacial, slipped benzene/benzene type between the two phenyls of the benzyl groups,[39,44] a benzene/benzene "T" interaction[45,46] between the phenyls of the benzyl and DPP groups and finally an electrostatically favorable interaction between the electronegative (carbonyl) O atom of one DPP core and the electropositive H atoms of the benzyl-methylene groups of the second DPP core in the $\pi-\pi$ dimer. The lower degree of benzyl-induced stabilization observed for ***ClBDPPβ*** is consistent with the slighter greater O···H atom as well as slipped cofacial $\pi-\pi$ benzene (benzyl) distances versus the ***HBDPP*** dimer pair originating from the larger Δx within the former dimer. There are two sets of each of these benzyl-based interactions per $\pi-\pi$ dimer.

The effect of the halo substitution on ΔE_{CP} can be teased out from examination of two pairs of results. The **XDPP** versus **DPP** results indicate slipped, cofacial halo-aryl/halo-aryl type interactions contribute a total of ∼10−20 kJ mol^{-1} toward ΔE_{CP} in the halo ***XBDPP*** dimers. Their contribution increases with increasing size of the halogen and the strength of such interactions show little variation between the α and β polymorphs (9.3 and 11.6 kJ mol^{-1} respectively) of ***ClBDPP***. Comparison of the ΔE_{CP} results for the ***XBDPP*** and **BDPP** $\pi-\pi$ dimers versus the **XDPP** and **DPP** indicates the role of benzyl-halo interactions in stabilizing the ***XBDPP*** $\pi-\pi$ dimers. "L" type close contacts between the electropositive phenyl hydrogen atoms of the benzyl groups and increasingly anisotropic electronegative X are observed in ***ClBDPPα***, ***BrBDPP***, and ***IBDPP*** $\pi-\pi$ dimers. These electrostatically driven halo-L-bonding "collar and cuff contacts" may be associated with a slight additional stability of ca. 3 and 5 kJ mol^{-1} for ***BrBDPP*** and ***IBDPP*** respectively over and above the apparently more dominant halo-aryl interactions also present. As anticipated by the lack of appropriate contacts in ***ClBDPPβ***, there is no indication of any additional stability conferred by such interactions in this case nor of significance in ***ClBDPPα***, where Δy = 1.2 Å is observed.

Both halo-aryl/halo-aryl type and benzyl based inter monomer contacts may therefore contribute significantly to the overall stability of the ***XBDPP*** $\pi-\pi$ dimer structures. Both interaction types appear to contribute to ΔE_{CP} of the short Δx slip halo $\pi-\pi$ dimer (***ClBDPPβ***) and the former to those $\pi-\pi$ dimers exhibiting longest Δx slippage (***BrBDPP***, ***IBDPP*** and ***ClBDPPα***). The sum of all of these halo and benzyl substituent associated interactions leads to enhancements of 10−30 kJ mol^{-1} in ΔE_{CP} for ***XBDPP*** versus **DPP** $\pi-\pi$ stacked dimers. It would therefore appear that benzyl substituents actively play an energetic role in the short molecular axis alignment of both ***HBDPP*** and ***ClBDPPβ*** monomers in forming the cofacial $\pi-\pi$ dimers as demonstrated by the results summarized in Table 2 and comparison with Δy observed in the crystal structures of nonbenzylated ***HDPP*** and ***ClDPP*** pigments. Their active role is less acute, although still favorable, in the halo-L-type electrostatic interactions contributing ∼3−5 kJ mol^{-1} to ΔE_{CP} of ***BrBDPP*** and ***IBDPP***. All of these ***XBDPP***s exhibit Δy < 0.5 Å. On the other hand, ***ClBDPPα*** has Δy = 1.2 Å and there is no evidence of the benzyl substituent conferring any stability to its $\pi-\pi$ dimer system.

In short, over and above any steric influence of benzylic substituents in restricting Δy, there is evidence for these groups enhancing the $\pi-\pi$ dimer binding energy in all ***XBDPP*** systems with Δy < 0.3 Å and no evidence of any energetic stability on ***ClBDPPα***. This is contrary to most DPP small molecules utilizing solubilizing *N*-alkyl groups,[43] and enforces the importance of N-benzyl substitution on facilitating cofacial alignment in DPP structures which *may* enhance charge transport in these particular crystalline DPP systems compared to others that have been published.

In effect, the ***XBDPP*** dimers in Figure 1C effectively represent a series of crystallographic "snap-shorts" taken over the course of a 1-D translation of one ***XBDPP*** monomer relative to the other over the long molecular axis. A natural question arises: what then are the underlying factors controlling ΔE_{CP} in DPP based $\pi-\pi$ dimer systems? This led us to generate a stacked **HDPP** cofacial $\pi-\pi$ dimer model at the M06-2X/6-31G(d) level. Starting from a fully *x*, *y* eclipsed structure with Δz = 3.6 Å, one monomer was translated relative to the second in 0.3 Å increments along *x*, keeping *y* and *z* constant. ΔE_{CP} of the dimer was computed at each increment.

Figure 4 shows the counter poise corrected M06-2X/631G(d) computed **HDPP** dimer interaction energy, ΔE_{CP}, as a function of Δx in red. Multiple minima in the resulting PES are observed corresponding to Δx = 1.5, 3.5, 5.1, 7.5, and 10.2 Å. The PES global minimum of 40 kJmol^{-1} is found at Δx = 3.5

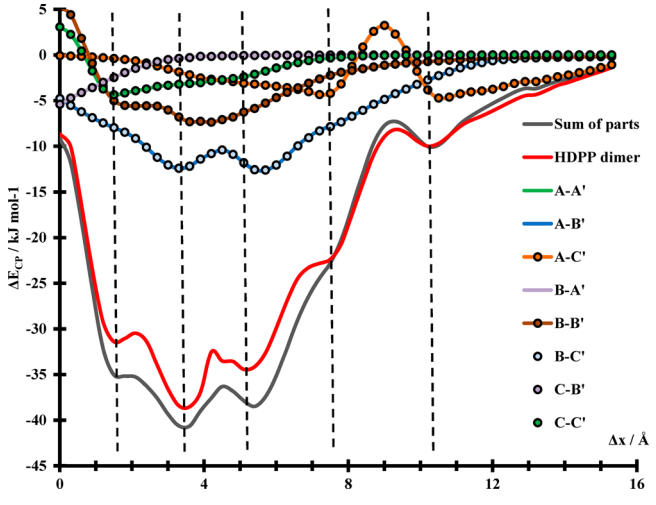

Figure 4. Counterpoise-corrected M06-2X/6-31G(d) **HDPP** model dimer interaction energy as a function of intermonomer slip, Δx.

dx.doi.org/10.1021/cg5010165 | *Cryst. Growth Des.* 2014, 14, 4849−4858

Å. The nature of the interactions responsible for the stability of cofacial $\pi-\pi$ dimer systems has been the focus of considerable attention in recent years[39,44,47−50] and the often quoted $\pi-\pi$ donor−acceptor interaction description[51] has been shown to be inadequate[39,44] at least in simple benzene based $\pi-\pi$ dimer systems. Instead, it would appear that cofacial $\pi-\pi$ stacks are primarily stabilized by local bond dipole/bond dipole and bond dipole induced interactions leading to slipped cofacial monomers with greater dimer stability than eclipsed.[39,44] As explained further below, our results as applied to the **HDPP** dimer summarized in Figure 4 are entirely consistent with this more recent viewpoint.

The **HDPP** dimer was broken up in to a series smaller dimer pairs; the phenyl rings on either side of the DPP core were labeled A(A′) and C(C′) with the DPP core as B(B′), where X/X′ indicate the units deriving from the upper and lower **HDPP** monomer respectively comprising the dimer. Thus, A−B−C represents the upper and A′−B′−C′ the lower monomer in the **HDPP** dimer. Then, each possible X/X′ pair originating from the dimer was subjected to a Δx shift from its original starting position within the dimer and ΔE_{CP} computed over the 15.5 Å translation. Thus, the A−A′ data represents movement of benzene ring A relative to its lower sibling, A′, over the Δx translation axis, A−B′ of the benzene ring translated over the lower DPP core and A-C′ of the upper benzene ring relative to the second benzene ring deriving from the lower dimer and so on as per Figure 4. This process introduces at least one new C−H bond per monomer in the newly generated dimer pair with respect to the original, parent **HDPP** dimer. There are a number of energetic equivalencies of the resulting X−X′ dimer pair interaction energies: A−A′ = C−C′, B−A′ = C−B′, and A−B′ = B−C′. The gray line in Figure 4 represents the sum of *all* of these subdimer ΔE_{CP}s.

*It is immediately apparent that positions of the local and global minima observed for the "intact" **HDPP** dimer are reproduced by the sum of the parts approach.* It therefore would appear that positions of local and global minima on the PES of the Δx translation in the **HDPP** dimer are not dependent on charge transfer interactions deriving from HOMO/LUMO π orbitals of the **HDPP** monomers as these have been broken up in the fragmentation process. On the other hand, if local bond dipole derived interactions contribute to the stability of the original **HDPP** dimer, increasing the number of C−H bond dipoles (as is implicit in this fragment based approach) ought to result in the sum of the parts PES curve being lower in energy than that of the original **HDPP** mode−as is the case here. This is by virtue of the "extra" C−H bonds created in capping the fragments of the original dimer. Indeed, repeating the above process using A, B and C over A′−B′-C′ results in a PES lying between the gray and red lines in Figure 4 although still coinciding with the local and global energy minima, as would be expected as the number of "extra" C−H bond dipoles is lower than with the X/X′ approach but still greater than in the **HDPP** dimers.

Figure 4 suggests that phenyl/DPP core, or A−B′ and B−C′ overlaps, make the greatest contribution to "$\pi-\pi$" dimer stability in diphenyl-substituted DPPs, with the remaining interactions superimposed on this PES. Observed Δx slips of 4.5 and 5.1 A in ***HBDPP*** and ***ClBDPPβ*** respectively coincide well with positions of local minima in the **HDPP** model (red) PES in Figure 4, as do the 9.4 A slips observed in ***ClBDPPα*** and ***IBDPP***. However, the ***BrBDPP*** Δx slip of 8.4 A does not coincide with a predicted **HDPP** minimum which, together with its lower total dimer interaction energy from all nearest neighbors *may* suggest that polymorphs with either greater, or lesser Δx slip may be possible under different crystal growth conditions. Indeed, the red PES in Figure 4 suggests that this may be true of all of the materials in this study. We are currently examining this further.

Taking all energetic results in to account, it would therefore appear that *all* of the interactions binding ***XBDPP*** "$\pi-\pi$"dimers together are local in nature. Each individual interaction may be relatively weak but in summation overall may lead to very large ΔE_{CP}s in "$\pi-\pi$" cofacial arrangements of DPPs. This conclusion is in contrast to recent postulations concerning such dimer energetics in other DPP systems.[43]

Charge Transfer Integrals, $t_{h/e}$. In view of the close alignment of the ***XBDPP*** crystal derived $\pi-\pi$ dimers along the x axis, we examined the variation of $t_{h/e}$ of the model **HDPP** model system with Δx within the framework of the energy splitting in dimer method[42] where t_h is given by half the energy splitting between the dimer HOMO and HOMO(−1) orbital pairs and likewise t_e by half the energy splitting between the LUMO and LUMO(+1) dimer orbital pair for centrosymmetric dimer pairs as we find in all cases here. The dependence of $t_{h/e}$ on Δx has previously been reported in a variety of $\pi-\pi$ dimer systems and is known to be a sensitive function of Δx in all of these systems.[20,21,42] However, the model results are the first one on DPPs, which is surprising given the increasing surge of interest in DPP-based materials and their application in optoelectronic systems.

When two monomeric π-conjugated molecules interact forming a $\pi-\pi$ cofacial dimer, supra-molecular dimer orbitals are generated from the linear combination of individual monomer orbitals. In particular, the in-phase addition of the individual DPP monomer HOMOs, namely η_a and η_b, gives rise to a new dimer orbital H_+ and the out of phase addition a new dimer orbital H_. At Δx = 0.0 (and Δy = 0.0, Δz = 3.6 Å), the fully bonding nature of the intermonomer interaction leads to H_ being lower in energy than H_+ which in turn exhibits fully antibonding character as illustrated in Figure 5. Upon Δx translation of 2.3 Å, the bonding and antibonding character of H_+ and H_ undergo complete reversal; now H_+ exhibits bonding (lower energy) and H_ antibonding (higher energy) character. The translation has led to the crossing of a nodal point at 1.5 Å. The interweaving of H_+/H_ orbital energies occurs over the entire Δx translation with a total of 5 nodal

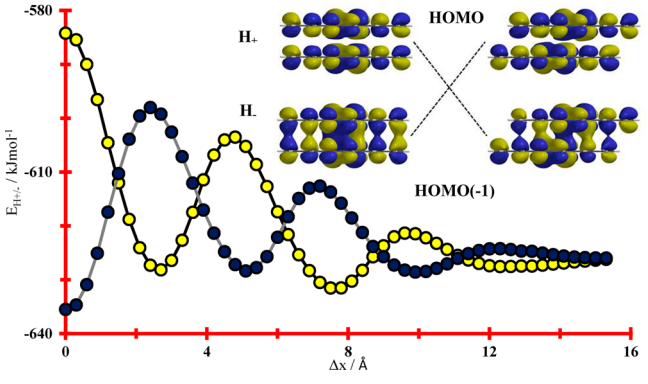

Figure 5. Plot of dimer orbital energies of H_+ (yellow) and H_ (blue) as a function of Δx. M06-2X/6-31G(d). Inset illustrates HOMOs of **HDPP** dimer at Δx = 0.0 (left) and 2.3 Å (right), Δy = 0.0 and Δz = 3.6 Å in both cases.

dx.doi.org/10.1021/cg5010165 | Cryst. Growth Des. 2014, 14, 4849−4858

points at positions corresponding to changes of sign in the original monomer HOMO orbital. A similar situation arises with the dimer L_+ and L_- orbital pairs generated from the linear combination of the monomer LUMOs, λ_a and λ_b, although now 6 nodes are generated, reflecting the extra node found in the monomer $\lambda_{a/b}$ orbitals.

The dependence of $1/2\Delta E_{H/L}$ on Δx for the model **HDPP** dimer system is given in Figure 6, in a form reflecting the

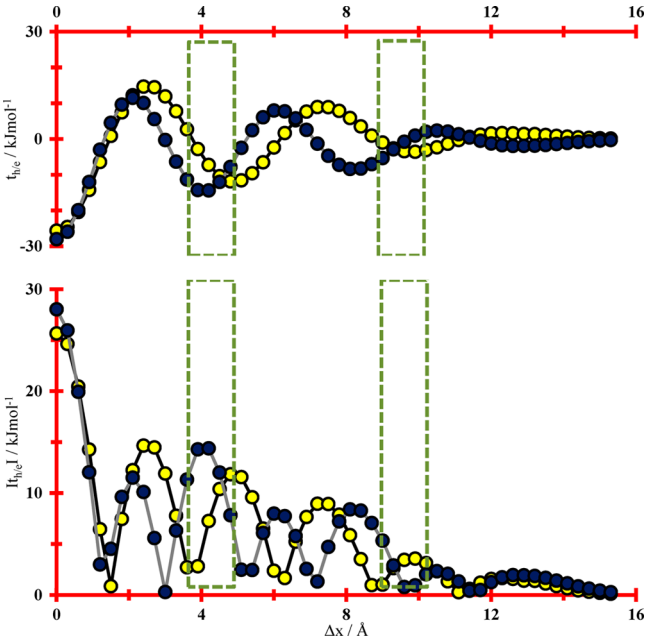

Figure 6. Hole (yellow) and electron (blue) transfer integral dependence on Δx for **HDPP** dimer system. Boxed regions indicate locations of minima in the dimer PES (Figure 4).

changing sign of t_h as a function of Δx (we define t_h as being given by $(E_{H_-} - E_{H_+})/2$ and likewise $t_e = (E_{L_-} - E_{L_+})/2$. As observed in a number of systems,[20,21,42] the resulting dependence of $t_{h/e}$ on Δx takes the form of a continuous, damped oscillation with maxima at $\Delta x = 0.0$ Å and their values vary substantially even over small variation in intermonomer translations. Looking at the dashed region in Figure 6, corresponding to the global minimum on the PES (~4.0 ± 1.4 Å) it can be seen that the absolute values of both t_h and t_e oscillate between values of ~9.5 and 0.0 kJ mol^{-1} over the range of Δx indicated. Furthermore, the relative magnitudes of t_h and t_e vary dramatically with respect to one another over this range; at 3.8 Å; $t_h \ll t_e$, at 4.6 Å; $t_h = t_e$, and at 5.2 Å; $t_h \gg t_e$. Similar behavior is observed over the broad local minimum at ~10 Å.

Subsequently, we determined $t_{h/e}$ for all the $\pi-\pi$ dimers in Figure 1. Computed $t_{h/e}$ values for the ***XBDPP*** $\pi-\pi$ dimers (as well as those related cropped dimers) are summarized in Table 3. In addition, the $t_{h/e}$ as well as $t^2_{h/e}$ (assuming band and hopping regimes respectively) results for the ***XBDPP*** series are shown in Figure 7.

We find that benzyl substituents do not influence $t_{h/e}$ values and that $t_{h/e}$ values of ***XBDPP*** versus **XDPP** and **BDPP** versus **DPP** pairs are essentially unchanged (<1 kJ mol^{-1} difference) on removal of the benzyl group. On the other hand, the presence of the additional halo-π lobes (2 per monomer) can be thought of as perturbing the $t_{h/e}$ values associated with the

Table 3. Computed Hole and Electron Transfer Integrals (t_h/t_e) for Structurally Modified and Non-Structurally Modified $\pi-\pi$ Dimer Pairs of Different N-Benzyl-Substituted DPP Derivatives[a]

	XBDPP (kJ mol^{-1})	XDPP (kJ mol^{-1})	BDPP (kJ mol^{-1})	DPP (kJ mol^{-1})
HBDPP	10.7/6.1	9.8/6.0	10.7/6.1	9.8/6.0
ClBDPPβ	11.8/4.0	11.4/3.8	12.8/2.5	12.4/2.4
BrBDPP	1.0/5.1	0.8/5.0	2.3/3.0	2.4/3.1
IBDPP	6.0/1.4	6.4/1.4	1.9/2.3	2.0/2.2
ClBDPPα	4.4/1.7	4.6/1.9	1.6/1.0	1.6/1.0
Rubrene	12.4/7.5			

[a]Non-structurally modified $\pi-\pi$ dimer pair of Rubrene included for comparison.

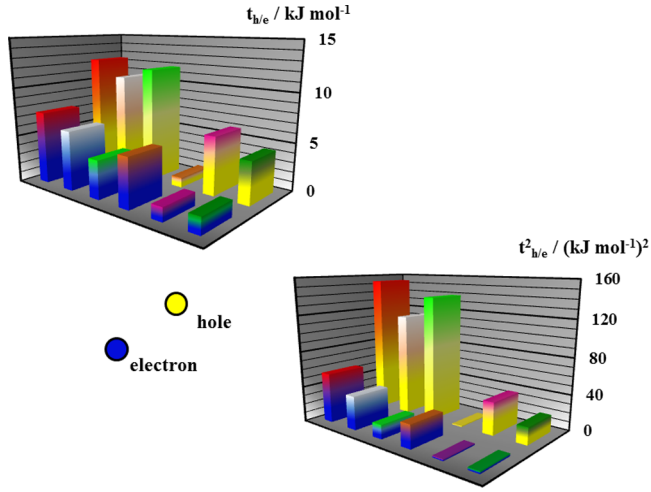

Figure 7. M06-2X/6-311G(d) computed hole (yellow base) and electron (blue base) charge transfer integrals (top left) and their square (bottom right) for extracted $\pi-\pi$ ***XBDPP*** dimers. Red topped, rubrene; white topped, ***HBDPP***; light green topped, ***ClBDPPβ***; brown, ***BrBDPP***; purple, ***IBDPP***; and dark green topped, ***ClBDPPα***.

DPP core (***XBDPP*** vs **BDPP** and **XDPP** vs **DPP**). In all but one instance (***IBDPP*** cropped structures) the relative ordering of t_h versus t_e in unaffected by the presence of the halo substituent although their individual values may be increased or decreased depending on how significantly the halo-π lobes perturb bonding/antibonding interaction in the H_+/H_- and L_+/L_- orbitals of the **HDPP** dimer.

Again with the exception of the ***IBDPP*** derived crops, we find that the relative ordering of t_h versus t_e of the DPP group matches that predicted by the model studies carried out in the **HDPP** dimer for the appropriate value of Δx. This is quite surprising given the lack of structural relaxation allowed in the model dimer system, most obviously with respect to the phenyl/DPP core torsional twist which is planar in the model.

The large t_h and t^2_h values of ***HBDPP*** and ***ClBDPPβ*** dominate both plots in Figure 7 with values approaching those of Rubrene and consistently exceed those we have computed for structurally related diketopyrrolopyrroles.[43,52,53] Thus, based on t_h, these two ***XBDPP***s like Rubrene, are expected to act as highly effective hole carriers along the dimer $\pi-\pi$ stacking axis in their crystalline state. Assuming semiconductor band-type behavior, the remaining $t_{h/e}$ values overall reflect comparable hole and electron transport properties over the group of remaining ***XBDPP***s with three exceptions; ***BrBDPP***

dx.doi.org/10.1021/cg5010165 | *Cryst. Growth Des.* 2014, 14, 4849−4858

favors electron transport by virtue of $t_e > t_h$ and hole transport is favored because of $t_h > t_e$ in both ***IBDPP*** and ***ClBDPPα***. Ambipolar electronic charge transport properties (although favoring hole transport) are associated with Rubrene, ***HBDPP*** and to a lesser extent ***ClBDPPβ***. On the other hand, thermal activated models of charge transport which depend on $t_{h/e}^2$, would suggest that hole mobility in ***HBDPP*** and ***ClBDPPβ*** dominates the overall electronically influenced charge transport properties of the ***XBDPP*** series.

Of particular note is that exchanging I for the Br atoms in ***BrBDPP*** results in a relative Δx shift of ∼1.0 Å between monomers in the ***IBDPP*** dimer. This 1.0 Å shift is responsible for a complete reversal of the relative ordering of the $t_{h/e}$ values between ***BrBDPP*** and ***IBDPP***; $t_e > t_h$ for ***BrBDPP***, whereas $t_h > t_e$ for ***IBDPP***. The relevant MOs of ***BrBDPP*** and ***IBDPP*** are given in Figure 8.

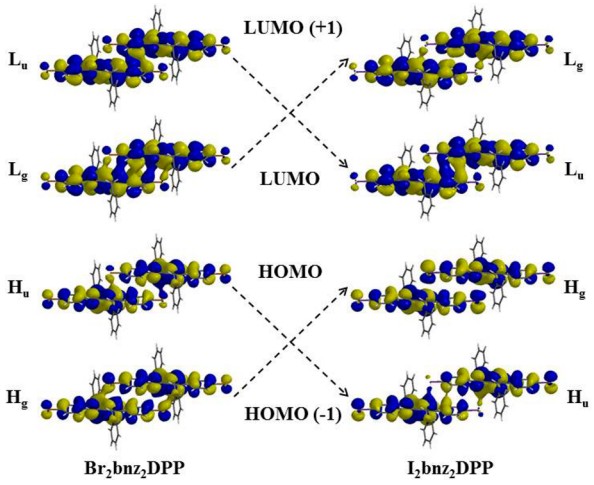

Figure 8. Kohn−Sham molecular orbitals of $\pi-\pi$ slipped, cofacial dimers of ***BrBDPP*** (left) and ***IBDPP*** (right). M06-2X/6-311G(d), IsoVal = 0.01.

The HOMO of ***BrBDPP*** is ungerade (H_u) and exhibits weak antibonding character. Applying a 1.0 Å shift of the upper monomer relative to the lower (as occurs in ***IBDPP***) results in a strong bonding interaction being generated in H_u, lowering its energy whereby it becomes the HOMO(−1) in ***IBDPP***. At the same time, the weakly bonding gerade orbital H_g (HOMO(−1)) in ***BrBDPP*** becomes strongly antibonding in ***IBDPP*** and as a result of the 1.0 Å shift, its energy is raised, now becoming the HOMO. The net result is that the energy splitting between H_u and H_g is considerably enhanced by the small shift in Δx leading to a greater t_h for ***IBDPP*** than ***BrBDPP*** (6.0 and 1.0 kJ mol^{-1} respectively). As illustrated in Figure 8, the opposite situation occurs in the LUMO/LUMO(+1) pairs; a 1.0 Å shift in Δx raises the energy of L_g while lowering that of L_u of ***BrBDPP*** resulting in a switching of their relative energies in ***IBDPP***. The bonding/antibonding character producing t_e = 5.1 kJ mol^{-1} for ***BrBDPP*** is reduced as a result of the small shift, giving 1.4 kJ mol^{-1} for ***IBDPP***. The observed switching in the relative t_h and t_e values associated with the 1.0 Å difference in Δx of the ***BrBDPP*** versus ***IBDPP*** crystal $\pi-\pi$ dimers is therefore entirely consistent with the extreme sensitivity of $t_{h/e}$ on Δx observed in the **HDPP** model herein and reported by others for different dimer systems.[20,21,42,54]

Overall, the various $t_{h/e}$ values determined for the ***XBDPP*** $\pi-\pi$ dimers can be rationalized on the basis of an underlying, systematic variation in the bonding/antibonding character in the HOMOs and LUMOs of an **HDPP** $\pi-\pi$ dimer associated with variation in Δx, subject to perturbation of the π-system by the two new π-lobes of the halo substituents on each monomer present.

CONCLUSIONS

In conclusion, 5 DPP-based crystal structures are reported, 4 of them novel, one of which is a new polymorph of a previously reported structure. All of these structures exhibit $\pi-\pi$ stacking motifs which run the length of the crystal. Local bond dipole and bond-dipole induced dipole interactions appear to stabilize these $\pi-\pi$ stacks as does the presence of both halo and benzyl substituents, the latter contributing significantly to Δx alignment of $\pi-\pi$ cofacial dimers in ***HBDPP*** and ***ClBDPPβ*** and to lesser extent in ***BrBDPP*** and ***IBDPP***.

We find that systematic variation of X in ***XBDPP***s leads to systematic variation in Δx (with little variation in Δy) and therefore in computed $t_{h/e}$ values for $\pi-\pi$ dimers extracted from the crystal structures, suggesting significant semiconductor bandwidth emerging along the crystallographic axis associated with the stacks. The resulting dependence of $t_{h/e}$ on Δx resembles that obtained from 1-D translation of one **HDPP** monomer versus another in a model system. The t_h values of ***HBDPP*** and ***ClBDPPβ*** $\pi-\pi$ dimers approach that of Rubrene, one of the most effective organic charge carrying crystalline materials reported to date. In addition, the binding energies of the ***HBDPP*** and ***ClBDPPβ*** $\pi-\pi$ dimers are significantly larger than the Rubrene dimer; $t_{h/e}$ values of the ***XBDPP*** pair may therefore show greater thermal resistance than those of the Rubrene $\pi-\pi$ dimer. The effect of polymorphism is clearly seen in a substantial lowering of both t_h and t_e in ***ClBDPPα*** relative to its ***β*** polymorph, highlighting the significance of polymorphism on the optimization of charge transfer properties in organic materials. The individual members of this systematically engineered crystal series of ***XBDPP***s differ from one another only in the nature of the 2X atoms substituted (out of 60 present), yet the resultant crystal structure variation induced is enough to produce large (10-fold) variation in $t_{h/e}$ to the extent that a complete switching of the predicted nature of the hole/electron mobility may be induced. In this sense, clear structure/predicted charge transfer integral relationships are evident which may be exploited by the development of crystalline organic electronic devices using these materials, rationally tailored to perform specific tasks. Such predicted relationships may also form the basis of systematic tests of charge transfer theory using ***XBDPP*** systems. Accordingly, we hope our report stimulates interest in these systems among the organic optoelectronic materials research community.

ASSOCIATED CONTENT

Supporting Information

Counterpoise corrected interaction energy, number of equivalent molecules, site and space-filled representation for all the nearest neighbor dimer pairs of ***XBDPP***s. X-ray crystallographic information files (CIF) are available for all of the reported structures. This material is available free of charge via the Internet at http://pubs.acs.org. Crystallographic information files are also available from the Cambridge Crystallographic Data Centre (CCDC) upon request (http://www.ccdc.cam.ac.uk), CCDC deposition numbers 980388−980392).

dx.doi.org/10.1021/cg5010165 | *Cryst. Growth Des.* 2014, 14, 4849−4858

AUTHOR INFORMATION

Corresponding Authors

*Tel: +44 (141) 848 3210. Fax: +44 (141) 848 3204. E-mail: callum.mchugh@uws.ac.uk.

*E-mail: andrew.mclean@uws.ac.uk. Tel: +44 (141) 848 3215

Notes

The authors declare no competing financial interest.

ACKNOWLEDGMENTS

C.J.M. and M.W. acknowledge EPSRC for funding under the First Grant Scheme EP/J011746/1, A.J.M. acknowledges PhD funding for J.C.-C. from UWS. The authors would like to thank Dr A. Marr, BASF, Paisley, for supply of DPP pigments and the NCS at the University of Southampton for crystallographic data collection on the ***ClBDPP*** and ***BrBDPP*** species.

REFERENCES

(1) Herbst, W.; Hunger, K. *Industrial Organic Pigments*; Wiley-VCH: Weinheim, Germany, 2004.

(2) Smith, H. M. *High Performance Pigments*; Wiley-VCH: Weinheim, Germany, 2002.

(3) Christie, R. M. *Colour Chemistry*; The Royal Society of Chemistry: Cambridge, U.K., 2001.

(4) Hong, W.; Sun, B.; Aziz, H.; Park, W.-T.; Noh, Y.-Y.; Li, Y. *Chem. Commun.* **2012**, *48*, 8413.

(5) Lee, J.; Cho, S.; Seo, J. H.; Anant, P.; Jacob, J.; Yang, C. *J. Mater. Chem.* **2012**, *22*, 1504.

(6) Chen, Z.; Lee, M. J.; Ashraf, R. S.; Gu, Y.; Albert-Seifried, S.; Nielsen, M. M.; Schroeder, B.; Anthopoulos, T. D.; Heeney, M.; McCulloch, I.; Sirringhaus, H. *Adv. Mater.* **2012**, *24*, 647.

(7) Cortizo-Lacalle, D.; Arumugam, S.; Elmasly, S. E. T.; Kanibolotsky, A. L.; Findlay, N. J.; Inigo, A. R.; Skabara, P. J. *J. Mater. Chem.* **2012**, *22*, 11310.

(8) Ha, J. S.; Kim, K. H.; Choi, D. H. *J. Am. Chem. Soc.* **2011**, *133*, 10364.

(9) Sonar, P.; Singh, S. P.; Li, Y.; Soh, M. S.; Dodabalapur, A. *Adv. Mater.* **2010**, *22*, 5409.

(10) Qu, S.; Qin, C.; Islam, A.; Wu, Y.; Zhu, W.; Hua, J.; Tian, H.; Han, L. *Chem. Commun.* **2012**, *48*, 6972.

(11) Qu, S.; Tian, H. *Chem. Commun.* **2012**, *48*, 3039.

(12) Qu, S.; Wu, W.; Hua, J.; Kong, C.; Long, Y.; Tian, H. *J. Phys. Chem. C* **2010**, *114*, 1343.

(13) Holcombe, T. W.; Yum, J.-H.; Yoon, J.; Gao, P.; Marszalek, M.; Di Censo, D.; Rakstys, K.; Nazeeruddin, M. K.; Graetzel, M. *Chem. Commun.* **2012**, *48*, 10724.

(14) Tamayo, A. B.; Dang, X.-D.; Walker, B.; Seo, J.; Kent, T.; Nguyen, T.-Q. *Appl. Phys. Lett.* **2009**, *94*, No. 103301.

(15) Tamayo, A. B.; Walker, B.; Nguyen, T.-Q. *J. Phys. Chem. C* **2008**, *112*, 11545.

(16) Loser, S.; Bruns, C. J.; Miyauchi, H.; Ortiz, R. P.; Facchetti, A.; Stupp, S. I.; Marks, T. J. *J. Am. Chem. Soc.* **2011**, *133*, 8142.

(17) Beaujuge, P. M.; Frechet, J. M. J. *J. Am. Chem. Soc.* **2011**, *133*, 20009.

(18) Mas-Torrent, M.; Rovira, C. *Chem. Rev.* **2011**, *111*, 4833.

(19) Wang, C.; Dong, H.; Hu, W.; Liu, Y.; Zhu, D. *Chem. Rev.* **2011**, *112*, 2208.

(20) Bredas, J. L.; Calbert, J. P.; da Silva, D. A.; Cornil, J. *Proc. Natl. Acad. Sci.U.S.A* **2002**, *99*, 5804.

(21) Coropceanu, V.; Cornil, J.; da Silva Filho, D. A.; Olivier, Y.; Silbey, R.; Bredas, J.-L. *Chem. Rev.* **2007**, *107*, 926.

(22) Wang, L.; Nan, G.; Yang, X.; Peng, Q.; Li, Q.; Shuai, Z. *Chem. Soc. Rev.* **2010**, *39*, 423.

(23) Troisi, A. *Chem. Soc. Rev.* **2011**, *40*, 2347.

(24) Atkins, P.; Friedman, R. *Molecular Quantum Mechanics*; Oxford University Press: Oxford, U.K., 2005.

(25) Kim, B. J.; Miyamoto, Y.; Ma, B.; Frechet, J. M. J. *Adv. Funct. Mater.* **2009**, *19*, 2273.

(26) Mizuguchi, J.; Grubenmann, A.; Rihs, G. *Acta Crystallogr., Sect. B* **1993**, *49*, 1056.

(27) Mizuguchi, J.; Grubenmann, A.; Wooden, G.; Rihs, G. *Acta Crystallogr., Sect. B* **1992**, *48*, 696.

(28) Kuwabara, J.; Yamagata, T.; Kanbara, T. *Tetrahedron* **2010**, *66*, 3736.

(29) MacLean, E. J.; Tremayne, M.; Kariuki, B. M.; Cameron, J. R. A.; Roberts, M. A.; Harris, K. D. M. *Cryst. Growth Des.* **2009**, *9*, 853.

(30) McGarry, K. A.; Xie, W.; Sutton, C.; Risko, C.; Wu, Y.; Young, V. G., Jr.; Bredas, J.-L.; Frisbie, C. D.; Douglas, C. J. *Chem. Mater.* **2013**, *25*, 2254.

(31) da Silva, D. A.; Kim, E. G.; Bredas, J. L. *Adv. Mater.* **2005**, *17*, 1072.

(32) Podzorov, V.; Menard, E.; Borissov, A.; Kiryukhin, V.; Rogers, J. A.; Gershenson, M. E. *Phys. Rev. Lett.* **2004**, *93*, No. 086602.

(33) Coles, S. J.; Gale, P. A. *Chem. Sci.* **2012**, *3*, 683.

(34) Sheldrick, G. M. *Acta Crystallogr., Sect. A* **2008**, *64*, 112.

(35) Shao, Y.; Molnar, L. F.; Jung, Y.; Kussmann, J.; Ochsenfeld, C.; Brown, S. T.; Gilbert, A. T. B.; Slipchenko, L. V.; Levchenko, S. V.; O'Neill, D. P.; DiStasio, R. A., Jr.; Lochan, R. C.; Wang, T.; Beran, G. J. O.; Besley, N. A.; Herbert, J. M.; Lin, C. Y.; Van Voorhis, T.; Chien, S. H.; Sodt, A.; Steele, R. P.; Rassolov, V. A.; Maslen, P. E.; Korambath, P. P.; Adamson, R. D.; Austin, B.; Baker, J.; Byrd, E. F. C.; Dachsel, H.; Doerksen, R. J.; Dreuw, A.; Dunietz, B. D.; Dutoi, A. D.; Furlani, T. R.; Gwaltney, S. R.; Heyden, A.; Hirata, S.; Hsu, C.-P.; Kedziora, G.; Khalliulin, R. Z.; Klunzinger, P.; Lee, A. M.; Lee, M. S.; Liang, W.; Lotan, I.; Nair, N.; Peters, B.; Proynov, E. I.; Pieniazek, P. A.; Rhee, Y. M.; Ritchie, J.; Rosta, E.; Sherrill, C. D.; Simmonett, A. C.; Subotnik, J. E.; Woodcock, H. L., III; Zhang, W.; Bell, A. T.; Chakraborty, A. K.; Chipman, D. M.; Keil, F. J.; Warshel, A.; Hehre, W. J.; Schaefer, H. F., III; Kong, J.; Krylov, A. I.; Gill, P. M. W.; Head-Gordon, M. *Phys. Chem. Chem. Phys.* **2006**, *8*, 3172.

(36) Boys, S. F.; Bernardi, F. *Mol. Phys.* **2002**, *100*, 65.

(37) Zhao, Y.; Truhlar, D. G. *Theor. Chem. Acc.* **2008**, *120*, 215.

(38) Vura-Weis, J.; Ratner, M. A.; Wasielewski, M. R. *J. Am. Chem. Soc.* **2010**, *132*, 1738.

(39) Wheeler, S. E. *Acc. Chem. Res.* **2013**, *46*, 1029.

(40) Allen, F. H. *Acta Crystallogr., Sect. B* **2002**, *58*, 380.

(41) Hablot, D.; Retailleau, P.; Ziessel, R. *Chem.—Eur. J.* **2010**, *16*, 13346.

(42) Bredas, J. L.; Beljonne, D.; Coropceanu, V.; Cornil, J. *Chem. Rev.* **2004**, *104*, 4971.

(43) Dhar, J.; Venkatramaiah, N.; Anitha, A.; Patil, S. *J. Mater. Chem. C* **2014**, *2*, 3457.

(44) Tauer, T. P.; Sherrill, C. D. *J. Phys. Chem. A* **2005**, *109*, 10475.

(45) Sinnokrot, M. O.; Sherrill, C. D. *J. Phys. Chem. A* **2004**, *108*, 10200.

(46) Sinnokrot, M. O.; Sherrill, C. D. *J. Am. Chem. Soc.* **2004**, *126*, 7690.

(47) Ehrlich, S.; Bettinger, H. F.; Grimme, S. *Angew. Chem., Int. Ed.* **2013**, *52*, 10892.

(48) Grimme, S. *Angew. Chem., Int. Ed.* **2008**, *47*, 3430.

(49) Antony, J.; Alameddine, B.; Jenny, T. A.; Grimme, S. *J. Phys. Chem. A* **2013**, *117*, 616.

(50) Martinez, C. R.; Iverson, B. L. *Chem. Sci.* **2012**, *3*, 2191.

(51) Hunter, C. A.; Sanders, J. K. M. *J. Am. Chem. Soc.* **1990**, *112*, 5525.

(52) Kim, C.; Liu, J.; Lin, J.; Tamayo, A. B.; Walker, B.; Wu, G.; Thuc-Quyen, N. *Chem. Mater.* **2012**, *24*, 1699.

(53) Liu, J.; Walker, B.; Tamayo, A.; Zhang, Y.; Thuc-Quyen, N. *Adv. Funct. Mater.* **2013**, *23*, 47.

(54) Kazmaier, P. M.; Hoffmann, R. *J. Am. Chem. Soc.* **1994**, *116*, 9684.